BIOCHEMISTRY
including biophysical chemistry & molecular biology

Article

pubs.acs.org/biochemistry

Kinetics Profiling of Gramicidin S Synthetase A, a Member of Nonribosomal Peptide Synthetases

Xun Sun,[†] Hao Li,[†] Jonas Alfermann,[‡] Henning D. Mootz,[‡] and Haw Yang*,[†]

[†]Department of Chemistry, Princeton University, Princeton, New Jersey 08544, United States

[‡]Institute of Biochemistry, University of Muenster, 48149 Münster, Germany

Supporting Information

ABSTRACT: Nonribosomal peptide synthetases (NRPS) incorporate assorted amino acid substrates into complex natural products. The substrate is activated via the formation of a reactive aminoacyl adenylate and is subsequently attached to the protein template via a thioester bond. The reactive nature of such intermediates, however, leads to side reactions that also break down the high-energy anhydride bond. The off-pathway kinetics or their relative weights compared to that of the on-pathway counterpart remains generally elusive. Here, we introduce multiplatform kinetics profiling to quantify the relative weights of on- and off-pathway reactions. Using the well-defined stoichiometry of thioester formation, we integrate a mass spectrometry (MS) kinetics assay, a high-performance liquid chromatography (HPLC) assay, and an ATP−pyrophosphate (PP_i) exchange assay to map out a highly efficient on-pathway kinetics profile of the substrate activation and intermediate uploading (>98% relative weight) for wide-type gramicidin S synthetase A (GrsA) and a 87% rate profile for a cysteine-free GrsA mutant. Our kinetics profiling approach complements the existing enzyme-coupled byproduct-release assays, unraveling new mechanistic insights of substrate activation/channeling in NRPS enzymes.

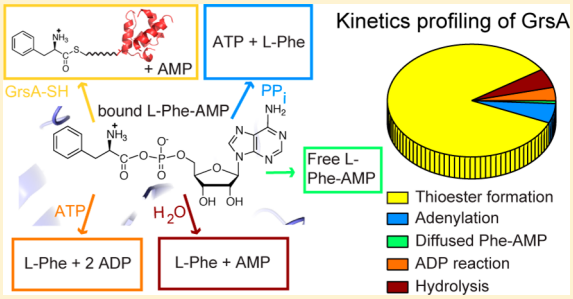

Nonribosomal peptide synthetases (NRPS) produce myriad life-saving natural products including potent antibiotics (e.g., penicillin) and anticancer drugs (e.g., bleomycin).[1] These hundreds-of-kilodalton enzymes are composed of distinct domains in a molecular assembly line manner, and each domain is responsible for catalyzing a distinct chemical transformation with a controlled timing to construct natural peptidyl products of remarkable chemical complexity (see Scheme 1A for gramicidin S synthetase A, GrsA, as an example).[2] It is precisely because NRPS function in such a modular way that they hold great promise for generating new drug-like molecules through combinatorial biosynthesis.[3,4] A thorough understanding of the reactivity of individual domains, as well as the assembly line as a whole, is expected to contribute to accelerating the discovery of new therapeutics.[5]

A minimal NRPS assembly line includes the following four domains: the adenylation domain (A) that activates a cognate amino acid, the peptidyl-carrier protein (PCP) that transfers the covalently attached aminoacyl motif along the assembly line, the condensation domain (C) that catalyzes the peptide bond formation, and the thioesterase domain (TE) that cleaves the product from the protein template.[6] The activation of various nonproteinogenic amino acid building blocks (>500 precursors[7]) by adenylation domains is achieved via a reactive acyl-adenylate (the adenylation step, cf. Scheme 1B).[8] This intermediate then forms a thioester bond with the free thiol group at the 4′-phosphopantetheine (Ppant) in the PCP domain (the thioesterification step, cf. Scheme 1B),[9] facilitating

Scheme 1. (A) Gene Cluster for the Biosynthesis of Gramicidin S[a] and (B) on/off Pathways of the Reactive Phenylalanyl Adenylate Intermediate for L-Phe Activation

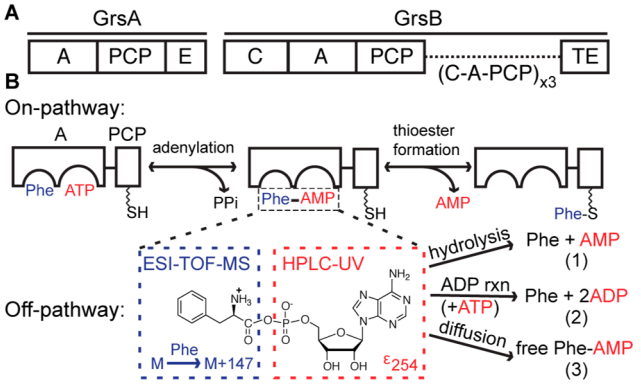

[a]E, epimerization domain (see text for other acronyms).

the downstream substrate channeling[10] at C, TE, and other possible tailoring domains.

To study the enzymatic reactivity along the multistep NRPS assembly process, a number of kinetic assays have been developed. For example, the ATP−PP_i exchange assay

Received: September 12, 2014
Revised: November 21, 2014
Published: December 1, 2014

characterizes the adenylation step in A domains,[11] and radioactive amino acid incorporation in PCP domains characterizes the thioester formation step.[12] These two assays directly measure the on-pathway kinetics. Here, the on pathway means the reaction pathway (both forward and reverse reactions) that leads to the final product that NRPS is supposed to produce. Assays have also been developed to study the dissociation of on-pathway byproducts. The enzyme-coupled PP_i assay characterizes adenylation byproduct release,[13] and the enzyme-coupled AMP assay characterizes thioester formation byproduct release.[14]

On the other hand, enzymes that synthesize reactive acyl-adenylate intermediates, including NRPS A domains and t-RNA synthetases, are also capable of catalyzing several off-pathway reactions (Scheme 1B), all of which involve breaking the high-energy anhydride bond (~15 kcal mol^{-1} estimated for carboxyl phosphate[15]). It was shown that, for t-RNA synthetases, the labile acyl-adenylate could react with ATP to form ADP,[16] with phosphate (P_i) to form ADP,[17] with PP_i to form ATP,[11] and with triphosphate (P_3) to form adenosine 5′-tetraphosphate.[18] Rapaport et al.[16] and Luo et al.[13] demonstrated the existence of the off-pathway side reaction of acyl adenylate with ATP in NRPS. Moreover, the acyl-adenylate could also be removed from the on-pathway reaction either by hydrolysis or by diffusion from the active site so that it becomes unavailable for making the final product. Despite these great advances in understanding the biochemistry of individual NRPS domains, the off-pathway kinetics or their relative weights in the overall reaction remains generally unknown.

Here, we put forward a multiplatform approach to address this general problem, and we illustrate the kinetics profiling idea with this approach by fully characterizing the kinetics profile of the bidomain GrsA A-PCP construct. As a model system in the NRPS family, the on-pathway kinetics of GrsA has been extensively studied using the previously mentioned radioactive kinetics assays[11,12,19] and the single-turnover analysis,[13,20] whereas the PP_i release kinetics has been reported as well.[13,20−22] In what follows, we outline our approach to elucidating the hitherto elusive kinetics profiles of on/off pathways of GrsA A-PCP. Its current form requires only facilities and instruments that are common to most institutes, including a radioactive lab, HPLC, and MS (Scheme 1B) for the ATP−PP_i exchange to probe the formation of acyl adenylate and its breakdown by PP_i, an MS kinetics assay to visualize the conversion of acyl adenylate to the thioester-bound holo protein, and an UV-HPLC kinetics assay to quantify the product formation in the remaining side reactions that consume the UV-sensitive acyl adenylate. Due to the micromolar detection limit of our UV-HPLC for adenosine (Figure S1), millimolar substrate and micromolar enzyme are mixed to allow micromolar product detection on the seconds-to-minute time scale; the high reactant concentrations also help to bias the forward reaction in these two-step reversible reactions. We note that the gross AMP formation measured by HPLC could come from (1) the off-pathway hydrolysis of acyl adenylate and (2) the on-pathway byproduct during thioesterification in holo proteins. To characterize the relative contributions from these two sources, we take advantage of the 1:1 stoichiometry of AMP and acyl-S-protein in thioester formation: AMP from source (2) could be calculated using the MS kinetics assay using such stoichiometry, and the rest of the AMP from source (1) can then be quantified. The MS-based approach is well-suited for this purpose; it naturally extends the micromolar substrate in the typical radiolabeling kinetics assay to millimolar substrate by using unlabeled substrates. In this work, we apply electrospray ionization time-of-flight MS (ESI-TOF-MS) without digestion or chromatographic separation for the MS kinetics assay of thioesterification in GrsA proteins. This approach expands the application scope of MS analysis from active site mapping[23] or substrate-loading visualization[24,25] to direct kinetics monitoring for NRPS proteins.

In this work, we carry out kinetics profiling for a wild-type (WT) A-PCP GrsA construct and contrast its profile against a previously reported Cys-free (CF) A-PCP construct that has a slightly reduced adenylation activity.[26] In that study, the CF mutant was engineered to enable the selective labeling of the thiol at Ppant, and the solvent accessibility of Ppant was investigated with various substrates. In this work, we choose CF as an example for evaluating the potential effect of the site-directed mutagenesis of engineered NRPS constructs. We quantitatively demonstrate that the kinetics changes from all monitored enzymatic reactions in CF compared to that in WT can be promptly reported via the kinetics profiling. Notably, our results underscore the efficient on-pathway reactivity in WT and CF constructs for both substrate activation (adenylation) and uploading (thioesterification).

EXPERIMENTAL PROCEDURES

Protein Expression, Purification, and Modification. Expression and purification of GrsA proteins were performed in a similar manner as previously reported,[26] with the modification that 10 mM $MgCl_2$ was supplemented during expression. *Escherichia coli* Rosetta (DE3) or BL21-Gold (DE3) was used as the expression strain. An extinction coefficient at 280 nm of 73 000 M^{-1} cm^{-1} was used to estimate the protein concentration. The apo-to-holo conversion was performed according to a protocol previously reported.[26] The molecular weight of purified or modified protein was determined by ESI-TOF-MS (Table S1). Unless otherwise noted, characterization experiments were carried out in 50 mM Tris/HCl, 300 mM NaCl, and 10 mM $MgCl_2$ (pH 8) at room temperature (25 °C). See Supporting Information for a detailed list of chemical materials used in this work.

HPLC Assay. HPLC experiments were performed in a 1260 HPLC machine (Agilent) with a reversed-phase column (dC18, 4.6 × 100 mm) with 3 μm particle size (Atlantic) and monitored at 254 nm. Running buffers A (more polar) and B (less polar) were prepared according to the work of Luo et al.[13] The elution gradient was set as follows: 0−2 min, 100% A; 2−25 min, 100% A to 33% A and 0% B to 67% B; 25−30 min, 33% A and 67% B, at a flow rate of 1 mL min^{-1}. Standards were used to identify the observed peak positions in the chromatograms, and concentration calibrations of AMP and L-Phe were performed (Figure S1). Seven micromolar apo or holo GrsA was incubated with 1 mM ATP and 1 mM L-Phe at room temperature for 30, 330, 630, and 930 s before the syringe filtering (0.2 μm Nylon) to remove the reactive enzyme from 60−70 μL of solution (Figure S2). Filtrates containing small molecules were kept on ice until being injected for HPLC analysis. HPLC peak areas were obtained using OpenLab Intelligent Reporting software (Agilent, A.01.06.111) with the default integration parameter setting.

ATP−PP_i Exchange Assay. Reactions were initiated by the addition of ATP and Phe (2 mM each) to a mixture of enzyme (300 nM), nonradioactive sodium pyrophosphate (0.2 mM), and 0.15 μCi of ^{32}P-labeled pyrophosphate in a final volume of

dx.doi.org/10.1021/bi501156m | Biochemistry 2014, 53, 7983−7989

100 μL. Experiments were conducted at 28 °C in NRPS assay buffer (50 mM 4-(2-hydroxyethyl)piperazine-1-ethanesulfonic acid (HEPES), 100 mM NaCl, 1 mM ethylenediaminetetraacetic acid (EDTA), and 20 mM $MgCl_2$, pH 7). The reaction was allowed to proceed for up to 15 min and then quenched by addition of a termination mixture (350 mM perchloric acid, 100 mM cold sodium pyrophosphate, 1.6% activated charcoal in water). Samples at 0 min were obtained by mixing protein and substrates directly in the termination mixture such that no reaction could occur. The quenched samples were mixed vigorously, incubated on ice for 1 min, and centrifuged for 1 min at 13 000 rpm (1 °C). Supernatant was removed, and charcoal pellets were washed twice by resuspending them in 800 μL of water and subsequent centrifugation. The pellet was finally resuspended in 500 μL of water and added to 2.5 mL of scintillation liquid (Aquasafe 500 plus, Zinsser Analytic GmbH). Scintillation counting was done by averaging counts over 1 min using a Beckman LS6500 multipurpose scintillation counter. All data points shown are the mean of at least two experiments conducted as triplicates. Experimental data performed with ∼1 μM supplemented PP_i is provided in Table S2.

MS Kinetics Assay. Purified protein was desalted using ZipTip (C18) pipet tips prior to MS analysis. For kinetics measurements, 2 μM enzyme was mixed with 1 mM ATP and 1 mM L-Phe at room temperature, and the sample was desalted at various time point for MS analysis. To desalt the protein sample, one solvent that is more polar (buffer C, 97% water, 3% acetonitrile, and 0.1% formic acid) and one that is less polar (buffer D, 90% acetonitrile, 10% water, and 0.1% formic acid) were used to desalt GrsA proteins. Desalting tips were first cleaned with 20 μL of buffer D twice and equilibrated with 20 μL of buffer C twice before use. On average, 2−20 μL of 0.3−10 μM protein was loaded into tips and washed in 20 μL of buffer C at least three times. Desalted protein was eluted in 9 μL of elution buffer (50% buffer C + 50% buffer D) for subsequent MS analysis. MS experiments were performed in a 6220 accurate-mass time-of-flight liquid chromatography/mass spectrometer (Agilent) in positive ion mode. The running buffer was 50% acetonitrile, 50% water, and 0.1% formic acid. The flow rate was 0.125 mL min^{-1}. The acquisition time was 711.9 ms/spectrum. For ESI-TOF setting, the gas temperature was 325 °C, V_{cap} was 350 V, the nebulizer pressure was set at 30 psig, the fragmentor voltage was 175 V, and the skimmer voltage was 65 V. The TOF mass window was set to be in the range of 100 to 1600 m/z. Raw mass data were analyzed using Mass Hunter software (Agilent, version B. 03.01, build 3.1.346.0) using a transformation algorithm proposed by Mann et al.[27] All multiply charged species were analyzed to obtain the mass of the parent species. The deconvoluted mass window was set to be from 55 000 to 80 000 Da. Standard compounds of purine ([M + H], 121.050873) and hexakis-(1H,1H,3H-tetrafluoropropoxy)phosphazine ([M + H], 922.009798) were used to calibrate mass measurements internally.

Thioester Formation ^{3}H Assay. ATP (1 mM), $MgCl_2$ (10 mM), and both cold and ^{3}H-labeled (175:1 ratio) Phe (4 μM) were preincubated at 25 °C in a bovine serum albumin (BSA)-coated reaction tube. The reaction was initiated by the addition of the enzymes (a final concentration of 300 nM), tris(2-carboxyethyl)phophine (TCEP, 5 mM), 50 mM HEPES, 100 mM NaCl, 1 mM EDTA, and 10 mM $MgCl_2$, pH 7 (^{3}H-assay buffer), to yield a final volume of 100 μL per sample. The reaction mixture was incubated at 25 °C, and samples of 100 μL were taken at specified time points. The reaction was quenched by the addition of 800 μL of ice-cold trichloroacetic acid (TCA, 10%) and 15 μL of BSA (25 mg mL^{-1}) to the reaction mixture. The protein fraction was precipitated by incubation on ice for 30 min and was subsequently centrifuged at 13 000 rpm for 30 min (1 °C). Pellets were washed with 800 μL of TCA (10%) twice to remove unbound substrates and redissolved in 150 μL of formic acid (98%). The solution was thoroughly mixed with 2.5 mL of liquid scintillation fluid, and radioactivity of the ^{3}H-labeled protein was determined by liquid scintillation counting, averaging over 5 min using a Beckman LS6500 multipurpose scintillation.

Profiling Data Analysis. The nonlinear kinetics of AMP formation in holo GrsA was described by the following equation

$$[\mathrm{AMP}(t)]_{\mathrm{holo}} = [\mathrm{Enz}](A - B\exp(k_{\mathrm{obs}}^{\mathrm{ESI}}t)) + [\mathrm{Enz}]k_{\mathrm{holo}}^{\mathrm{hydro}}t \quad (1)$$

where the single-exponential component in first term is from ESI-TOF-MS experiments (Figure S15), $k_{\mathrm{holo}}^{\mathrm{hydro}}$ is the time constant for Phe-AMP hydrolysis in holo enzymes, and [Enz] is the enzyme concentration. This is the key equation that integrates the HPLC and ESI-TOF-MS measurements.

The remaining product formation kinetics was found to be linear within the first 15 min of the reaction; therefore, these kinetics data were fit to a zero-order kinetic model

$$[\mathrm{product}(t)] = [\mathrm{Enz}]kt + C \quad (2)$$

where k is the rate constant for corresponding reaction and C is a fitting parameter. We then normalized the linear slope ([Enz] k, μM s^{-1}) of product formation using the GrsA protein concentration to obtain rate constant (s^{-1}) in a similar manner as previously reported.[28] Since all enzymatic reactions involve the Phe-AMP intermediate, the overall observed rate of Phe-AMP ($k_{\mathrm{apo/holo}}^{\mathrm{PheAMP}}$) can be expressed by

$$k_{\mathrm{apo/holo}}^{\mathrm{PheAMP}} = k_{\mathrm{apo/holo}}^{\mathrm{hydro}} + \frac{1}{2}k_{\mathrm{apo/holo}}^{\mathrm{ADP}} + k_{\mathrm{obs}}^{\mathrm{ESI}} + k_{\mathrm{apo/holo}}^{\mathrm{loss}} + k_{\mathrm{apo/holo}}^{\mathrm{PPi}} \quad (3)$$

where $k_{\mathrm{apo/holo}}^{\mathrm{hydro}}$ is the Phe-AMP hydrolysis rate, $k_{\mathrm{apo/holo}}^{\mathrm{ADP}}$ is the rate of the ADP side reaction, $k_{\mathrm{obs}}^{\mathrm{ESI}}$ is the Ppant modification rate from ESI-TOF-MS (0 for apo protein), $k_{\mathrm{apo/holo}}^{\mathrm{loss}}$ is the net release rate of diffused Phe-AMP, and $k_{\mathrm{apo/holo}}^{\mathrm{PPi}}$ is the rate for the adenylation reaction. The factor of 2 comes from the stoichiometry of ATP in this ADP side reaction (Scheme 1B(2)). See the Supporting Information for more detailed analysis and additional experimental methods. Unless otherwise noted, experiments were independently performed three times, and results are reported as the mean ± 1 standard deviation, analyzed using MATLAB (Mathworks, R2013a).

RESULTS AND DISCUSSION

Kinetics Profiling of Apo Proteins. We first established an HPLC protocol to monitor UV-sensitive small molecules (AMP, ADP, and Phe) at 254 nm to quantify their concentrations in the micro- to millimolar range (Figures S1 and S2). Under our experimental conditions, Phe-AMP remained stable (Figure S3A). We then measured the kinetics of apo WT/CF (Figure 1A) using HPLC/ATP−PP_i exchange. Linear kinetics of AMP, ADP, and Phe-AMP was clearly shown by HPLC (Figures 1B−1D). The formation of such products

dx.doi.org/10.1021/bi501156m | Biochemistry 2014, 53, 7983−7989

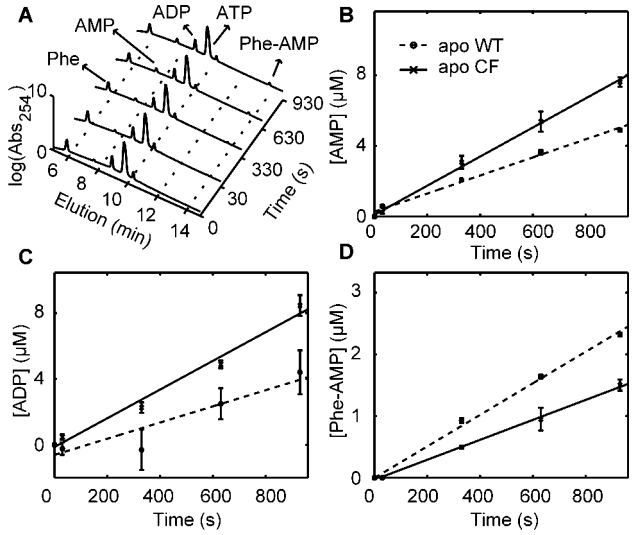

Figure 1. HPLC analysis of side reactions in apo WT/CF GrsA. (A) Representative time-dependent HPLC traces of apo WT with ATP + L-Phe. The absorbance is shown on a log scale. (B–D) Linear kinetics of AMP (B), ADP (C), and diffused Phe-AMP formation (D) in apo WT (dash fitting line) and in apo CF (solid fitting line). Error bars represent 1 standard deviation from three repeats.

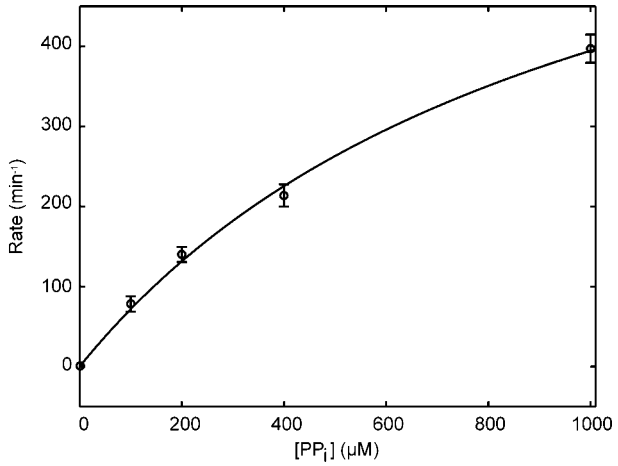

Figure 2. Rate of adenylation depends on the PP_i concentration for apo WT. A Henri–Michaelis–Menten-type equation is used to fit the adenylation rate data at different PP_i concentrations. Error bars represent 1 standard deviation from at least three repeats.

was assumed to be dependent on the enzymatic reaction because ATP plus L-Phe was stable at room temperature for a time span longer than that of the HPLC run without enzyme (Figure S3B) and because the omission of L-Phe led to no newly formed AMP, ADP, or Phe-AMP, given the micromolar detection limit of our HPLC for the adenosine-bearing motif (Figure S4). Due to the absence of the on-pathway byproduct AMP from thioesterification in the apo enzyme without the background Ppant modification during expression (Figure S5), all AMP in this experiment was assumed to be from the off-pathway hydrolysis of Phe-AMP (Scheme 1B(1)). ADP presumably is from the off-pathway side reaction of Phe-AMP and ATP (Scheme 1B(2)), whereas the observed free Phe-AMP probably dissociates from its binding pocket within the A domain (another off pathway in Scheme 1B(3)). For the on-pathway adenylation reaction, we observed Henri–Michaelis–Menten-type kinetics depending on the supplemented PP_i concentration (Figure 2), suggesting that the sum of forward and reverse adenylation is proportional to the supplemented PP_i concentration when the latter is far smaller than the Michaelis–Menten constant. We then estimated the PP_i concentration in the HPLC assay and used it to estimate the rate of adenylation (see details in the Supporting Information). As expected, the rate of the on-pathway adenylation reaction in apo WT contributes ~80% of the overall rate. This on-pathway kinetics weight is reduced to ~55% in apo CF (Table 1; see the Supporting Information for kinetics equations and quantifications).

Verification of the MS Assay. Since the MS kinetics assay was needed to quantify the kinetics of holo WT and holo CF, we first proceeded to verify the accuracy of our ESI-TOF-MS assay for the 70 kDa GrsA constructs and obtained correct molecular weights compared to calculated ones for both apo and holo proteins with or without aminoacyl modification (Table S1 and Figure S5 and S6). We also confirmed the stability of Phe-S-protein (M + 147) under our experimental conditions (Figure S7). As expected, aminoacylation was ATP-dependent in holo constructs and completed within 10 min at room temperature for both holo proteins (Figure S6). By contrast, incubating apo WT/CF with both substrates for 1 h did not result in the Phe-adduct peak, consistent with the swinging-arm model[29,30] in which the Ppant attached to the arguably highly mobile holo PCP is rapidly aminoacylated in our MS kinetics assay (Figure S8). Interestingly, we observed autoaminoacylations with multiple covalent L-phenylalaminoacyl adducts (M + 147x, x = 1, 2, ...) in incubations taking place over a span of days, analogous to what has been observed for several tRNA synthetases.[31,32]

Having confirmed the measurement accuracy and stability of acyl-S-protein under our experimental conditions, we set out to validate our MS-based kinetics method by comparing it to the standard radiolabeling assay. We first manually desalted holo CF from ATP/L-Phe at various time points within a 15 min reaction time window. A series of time-dependent mass spectra clearly showed the conversion from free holo CF to Phe-loaded holo CF (Figure 3A). As demonstrated by the pioneering work of the Kelleher group, an accuracy of ~5% error in estimating relative protein concentrations could be achieved for (un)-modified full-length GrsA ionized via ESI.[24] We normalized the percentages of L-Phe-loaded protein using the deconvoluted mass peak heights.[27] We then obtained the thioester formation kinetics from a first-order kinetics model ($(4.7 \pm 0.9) \times 10^{-3}$ s^{-1}, cf. Figure 3B) that was in quantitative agreement with the standard L-[^{3}H]-Phe assay under the same experimental conditions ($(4.2 \pm 0.1) \times 10^{-3}$ s^{-1}, cf. Figure S9). In contrast, thioester formation of holo WT was complete within 6 s at room temperature (Figure S6), in agreement with a previous report on full-length GrsA using the radioactive assay.[19] A ~10-fold increase in the L-Phe binding constant (K_d) (Figure S10) and a less compact global conformation (Figures S11–S12) may account for the observed slower rate of interdomain thioester formation in holo CF. Nevertheless, these results allowed a lower bound to be determined for the thioester formation kinetics in holo WT with saturating substrate (Figure S13).

Kinetics Profiling of Holo Proteins. After establishing the suitability and accuracy of HPLC and MS kinetics experiments, we next performed full kinetics profiling for holo WT and CF proteins. Within a 15 min incubation at room temperature, HPLC analysis clearly demonstrated linear kinetics of ADP and

dx.doi.org/10.1021/bi501156m | Biochemistry 2014, 53, 7983–7989

Table 1. Kinetics Profiling of Apo/Holo WT/CF GrsA A-PCP Constructs with Saturated ATP/L-Phe

rate (s^{-1})	AMP-forming hydrolysis	ADP-forming reaction	Phe-AMP diffusion	adenylation reaction	thioesterification reaction	sum of rates
Apo WT	$(7.2 \pm 0.1) \times 10^{-4}$	$(3.9 \pm 1.3) \times 10^{-4}$	$(3.6 \pm 0.1) \times 10^{-4}$	$(6.2 \pm 0.8) \times 10^{-3}$	0	$(7.7 \pm 0.8) \times 10^{-3}$
Apo CF	$(1.2 \pm 0.1) \times 10^{-3}$	$(6.2 \pm 0.6) \times 10^{-4}$	$(2.3 \pm 0.2) \times 10^{-4}$	$(2.6 \pm 0.2) \times 10^{-3}$	0	$(4.7 \pm 0.2) \times 10^{-3}$
Holo WT	$(6.0 \pm 0.1) \times 10^{-4}$	$(3.1 \pm 0.3) \times 10^{-4}$	$(1.8 \pm 0.4) \times 10^{-4}$	$(4.9 \pm 0.4) \times 10^{-3}$	$>5.8 \times 10^{-2}$	$>6.4 \times 10^{-2}$
Holo CF	$(5.9 \pm 2.2) \times 10^{-4}$	$(4.1 \pm 2.1) \times 10^{-4}$	$(8.7 \pm 2.3) \times 10^{-5}$	$(0.6 \pm 0.1) \times 10^{-3}$	$(9.0 \pm 1.4) \times 10^{-3}$	$(1.1 \pm 0.1) \times 10^{-2}$

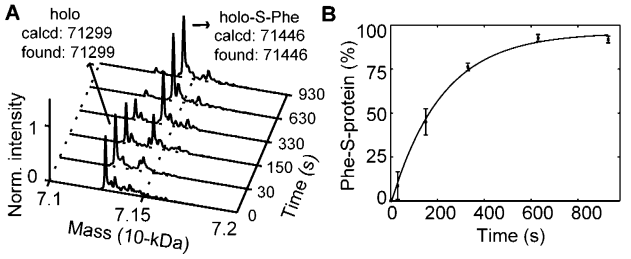

Figure 3. ESI-TOF-MS kinetics assay for holo CF with micromolar Phe. (A) Representative mass traces showing the conversion from holo CF to Phe-S-protein. (B) Kinetics of the thioester formation reaction. Error bars are 1 standard deviation from three repeats.

Phe-AMP formation for holo CF (Figures 4B,C and S14). In contrast, nonlinear AMP formation kinetics was observed

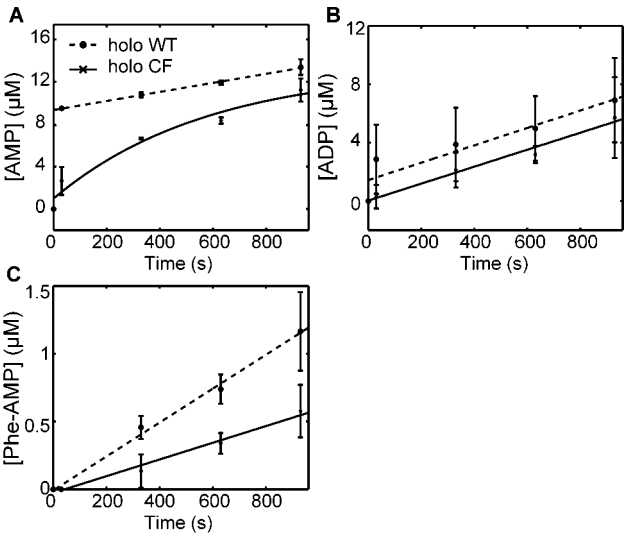

Figure 4. HPLC analysis of holo WT/CF GrsA. Kinetics of AMP (A), ADP (B), and Phe-AMP (C) in holo WT (dashed line) and in holo CF (solid line). Error bars represent 1 standard deviation from three repeats.

(Figure 4A). This result was expected because the sum of first-order thioester formation (Figure S15) and zero-order hydrolysis (with respect to the enzyme) could give rise to nonlinear AMP formation. Taken together, the kinetics profile of holo CF showed an ~82% weight for thioester formation and an ~87% weight for both adenylation and thioesterification (Table 1). In the case of holo WT, the lower bound of the relative weight was 91% for thioester formation and 98% for both adenylation and thioester formation. Interestingly, the nonlinear kinetics feature of holo CF AMP formation was clearly absent in holo WT (Figure 4A); this is because the first-order thioester formation was completed before the first HPLC time point (30 s) and only the linear Phe-AMP hydrolysis was monitored post thioesterification. Furthermore, due to the rapid formation of one equivalent of AMP (~7 μM), the AMP concentration in holo WT at the first time point (30 s) was expected to be much higher than that of its apo or CF counterpart (~2−3 μM). Indeed, it was shown via HPLC analysis of holo WT that this is the case (Figure 4A). Similar to apo CF/WT, linear kinetics of ADP and Phe-AMP was observed for holo WT.

Collectively, these kinetics profiling experiments clearly indicated that, with excess substrates, holo WT GrsA keeps consuming acyl-adenylate intermediates, but it does so at a slower rate after the completion of Ppant aminoacylation. Such kinetics, manifested by a rapid initial burst followed by a slower increase, has also been observed in homologous enzymes.[14,28,33] Furthermore, our profiling may provide a kinetic basis for previous reports in which a second equivalent of the cognate amino acid and ATP can be consumed before Ppant is discharged again:[33,34] although tight binding between the second equivalent of acyl-adenylate and the NRPS A domain as well as the loaded Ppant may inhibit the next round's on-pathway reaction, all of the off-pathway reactions (Scheme 1B(1−3)) could still occur post-thioesterification. These concurrently occurring off-pathway reactions consume the second equivalent acyl-adenylate intermediate at a much slower summed rate (at least 53-fold reduced compared to thioesterification in holo WT), as first reported here, ensuring the observed 2× stoichiometry in the substrate consumption. Conceivably, the breakdown of the enzyme−intermediate complex post-thioesterification to recover the free enzyme capable of reinitiating another round of catalysis is a slow step, if not the rate-limiting one. Similarly, the profiled WT holo kinetics is also consistent with the finding that only one equivalent of AMP can be measured[35] due to the negligible off-pathway acyl-adenylate hydrolysis rate compared to the on-pathway thioester formation rate (Table 1).

Mechanistically, the observed highly efficient on-pathway kinetics profile of thioester formation in the GrsA A-PCP bidomain construct can be attributed to the higher nucleophilicity of the sulfur at Ppant as compared to the oxygen in solvents or competing substrates; it also suggests that the labile Phe-AMP is well-protected while it waits to be channeled by the mobile Ppant in PCP, presumably in certain catalytic conformation(s). Kinetic models incorporating two alternating catalytic conformations have been proposed,[14,28,36] yet the detailed interplays between conformation and chemistry in NRPS warrant further investigations.

CONCLUSIONS

In this work, we have demonstrated an integrated, multiplatform enzymatic kinetics profiling approach to quantify chemical reactions associated with the reactive acyl-adenylate in NRPS A-PCP domains. We showcase one of its immediate applications by revealing highly efficient adenylation−thioesterification with the WT GrsA A-PCP construct. Local perturbations, as illustrated here by amino acid substitutions in the CF mutant protein, can lead to deviations from this highly optimized pathway. This point should be considered in

dx.doi.org/10.1021/bi501156m | Biochemistry 2014, 53, 7983−7989

future biocombinatorial approaches using engineered NRPS. Technically, such kinetics profiling well complements other established enzymatic assays, such as the enzyme-coupled assays for PP_i and AMP release, enabling a comprehensive kinetics perspective for NRPS systems. It is noteworthy that the kinetics profiling approach as reported here could be expanded to measure fast kinetics processes when coupled with a rapid-quenching apparatus. Indeed, on the basis of the success of the present work, one could envision other ways of profiling the kinetics of a molecular assembly line so long as the approach conforms to the following attributes: (a) the method must be able to simultaneously follow the time course of many, ideally all, reactants, intermediates, and products; (b) if more than one method is used in profiling, then data from different sources must be quantitatively integrated; and (c) cross-validation for results from different sources must be performed whenever possible. We anticipate that the kinetics profiling idea will offer a valuable readout when investigating the molecular basis for such highly efficient on-pathway kinetics in NRPS A-PCP domains or other homologous adenylation protein families.

■ ASSOCIATED CONTENT

Supporting Information

Experimental methods. Table S1: Protein mass measured by ESI-TOF-MS. Table S2: ATP−PP_i exchange assay results. Figure S1: HPLC calibrations. Figure S2: Filtering to remove protein sample. Figure S3: Chemical stability verified by HPLC. Figure S4: Formation of Phe-AMP is dependent on L-Phe. Figure S5: Apo-holo conversion probed by MS. Figure S6: Substrate loading by ESI-TOF-MS. Figure S7: Phe-S-protein stability confirmed by ESI-TOF-MS. Figure S8: Multiple aminoacylation in apo/holo GrsA. Figure S9: Radioactive ^{3}H-Phe loading measurements. Figure S10: Dissociation constant of L-Phe in apo GrsA. Figure S11: Native gel analysis for GrsA with the Phe-AMS inhibitor. Figure S12: Trypsin digestion experiments to probe the surface-exposable linker between (sub)domains. Figure S13: Fast ^{3}H-Phe uploading in holo WT. Figure S14: HPLC analysis for holo WT/CF GrsA. Figure S15: Holo CF kinetics with saturated substrates. Figure S16: Thioester formation of holo WT-C331A. This material is available free of charge via the Internet at http://pubs.acs.org.

■ AUTHOR INFORMATION

Corresponding Author

*E-mail: hawyang@princeton.edu. Telephone: +1(609)-258-3578.

Funding

This work was supported by Human Frontiers Science Program award no. RGP0031/2010-C202. Financial support from the University of Muenster and Princeton University is also gratefully acknowledged.

Notes

The authors declare no competing financial interest.

■ ACKNOWLEDGMENTS

We thank J. Eng for technical assistance with the ESI-TOF-MS experiments, J. Diecker for technical assistance with the radioactive assays, and D. Fiedler for the use of the HPLC.

■ ABBREVIATIONS

A, adenylation; C, condensation; CF, cysteine-free; ESI-TOF-MS, electrospray ionization time-of-flight mass spectrometry; GrsA, gramicidin S synthetase A; HPLC, high-performance liquid chromatography; NRPS, nonribosomal peptide synthetase; PCP, peptidyl carrier protein; Phe-AMP, phenylalanyl-adenosine-5′-phosphate diester; PP_i, pyrophosphate; TE, thioesterase; WT, wild type

■ REFERENCES

(1) Felnagle, E. A., Jackson, E. E., Chan, Y. A., Podevels, A. M., Berti, A. D., McMahon, M. D., and Thomas, M. G. (2008) Nonribosomal peptide synthetases involved in the production of medically relevant natural products. *Mol. Pharmaceutics 5*, 191−211.

(2) Fischbach, M. A., and Walsh, C. T. (2006) Assembly-line enzymology for polyketide and nonribosomal peptide antibiotics: logic, machinery, and mechanisms. *Chem. Rev. 106*, 3468−3496.

(3) Mootz, H. D., Schwarzer, D., and Marahiel, M. A. (2000) Construction of hybrid peptide synthetases by module and domain fusions. *Proc. Natl. Acad. Sci. U.S.A. 97*, 5848−5853.

(4) Nguyen, K. T., Ritz, D., Gu, J. Q., Alexander, D., Chu, M., Miao, V., Brian, P., and Baltz, R. H. (2006) Combinatorial biosynthesis of novel antibiotics related to daptomycin. *Proc. Natl. Acad. Sci. U.S.A. 103*, 17462−17467.

(5) Cane, D. E., Walsh, C. T., and Khosla, C. (1998) Harnessing the biosynthetic code: combinations, permutations, and mutations. *Science 282*, 63−68.

(6) Marahiel, M. A., Stachelhaus, T., and Mootz, H. D. (1997) Modular peptide synthetases involved in nonribosomal peptide synthesis. *Chem. Rev. 97*, 2651−2674.

(7) Caboche, S., Leclère, V., Pupin, M., Kucherov, G., and Jacques, P. (2010) Diversity of monomers in nonribosomal peptides: towards the prediction of origin and biological activity. *J. Bacteriol. 192*, 5143−5150.

(8) Berg, P. (1956) Acyl adenylates: an enzymatic mechanism of acetate activation. *J. Biol. Chem. 222*, 991−1013.

(9) Stein, T., Vater, J., Kruft, V., Otto, A., Wittmann-Liebold, B., Franke, P., Panico, M., McDowell, R., and Morris, H. R. (1996) The multiple carrier model of nonribosomal peptide biosynthesis at modular multienzymatic templates. *J. Biol. Chem. 271*, 15428−15435.

(10) Wu, N., Tsuji, S. Y., Cane, D. E., and Khosla, C. (2001) Assessing the balance between protein-protein interactions and enzyme−substrate interactions in the channeling of intermediates between polyketide synthase modules. *J. Am. Chem. Soc. 123*, 6465−6474.

(11) Gevers, W., Kleinkauf, H., and Lipmann, F. (1968) The activation of amino acids for biosynthesis of gramicidin S. *Proc. Natl. Acad. Sci. U.S.A. 60*, 269−276.

(12) Stachelhaus, T., and Marahiel, M. A. (1995) Modular structure of peptide synthetases revealed by dissection of the multifunctional enzyme GrsA. *J. Biol. Chem. 270*, 6163−6169.

(13) Luo, L., and Walsh, C. T. (2001) Kinetic analysis of three activated phenylalanyl intermediates generated by the initiation module PheATE of gramicidin S synthetase. *Biochemistry 40*, 5329−5337.

(14) Wu, R., Cao, J., Lu, X., Reger, A. S., Gulick, A. M., and Dunaway-Mariano, D. (2008) Mechanism of 4-chlorobenzoate:coenzyme A ligase catalysis. *Biochemistry 47*, 8026−8039.

(15) Lipmann, F. (1944) Enzymatic synthesis of acetyl phosphate. *J. Biol. Chem. 155*, 55−70.

(16) Rapaport, E., Remy, P., Kleinkauf, H., Vater, J., and Zamecnik, P. C. (1987) Aminoacyl-tRNA synthetases catalyze AMP→ADP→ATP exchange reactions, indicating labile covalent enzyme-amino-acid intermediates. *Proc. Natl. Acad. Sci. U.S.A. 84*, 7891−7895.

(17) Guédon, G., Ebel, J. P., and Remy, P. (1987) Yeast phenylalanyl-tRNA synthetase: evidence for the formation of ADP by phosphorolysis of enzyme-bound aminoacyladenylate. *Biochimie 69*, 1175−1181.

(18) Güranowski, A., Sillero, M. A. G., and Sillero, A. (1994) Adenosine 5′-tetraphosphate and adenosine 5′-pentaphosphate are

synthesized by yeast acetyl-coenzyme-A synthetase. *J. Bacteriol. 176*, 2986−2990.
(19) Stachelhaus, T., Mootz, H. D., Bergendahl, V., and Marahiel, M. A. (1998) Peptide bond formation in nonribosomal peptide biosynthesis—catalytic role of the condensation domain. *J. Biol. Chem. 273*, 22773−22781.
(20) Luo, L., Burkart, M. D., Stachelhaus, T., and Walsh, C. T. (2001) Substrate recognition and selection by the initiation module PheATE of gramicidin S synthetase. *J. Am. Chem. Soc. 123*, 11208−11218.
(21) Chen, C. Y., Georgiev, I., Anderson, A. C., and Donald, B. R. (2009) Computational structure-based redesign of enzyme activity. *Proc. Natl. Acad. Sci. U.S.A. 106*, 3764−3769.
(22) Stevens, B. W., Lilien, R. H., Georgiev, I., Donald, B. R., and Anderson, A. C. (2006) Redesigning the PheA domain of gramicidin synthetase leads to a new understanding of the enzyme's mechanism and selectivity. *Biochemistry 45*, 15495−15504.
(23) Stein, T., Vater, J., Kruft, V., Wittmannliebold, B., Franke, P., Panico, M., Mcdowell, R. M., and Morris, H. R. (1994) Detection of 4′-phosphopantetheine at the thioester binding-site for L-valine of gramicidins synthetase-2. *FEBS Lett. 340*, 39−44.
(24) Miller, L. M., Mazur, M. T., McLoughlin, S. M., and Kelleher, N. L. (2005) Parallel interrogation of covalent intermediates in the biosynthesis of gramicidin S using high-resolution mass spectrometry. *Protein Sci. 14*, 2702−2712.
(25) Hicks, L. M., Mazur, M., Miller, L. M., Dorrestein, P. C., Schnarr, N. A., Khosla, C., and Kelleher, N. L. (2006) Investigating nonribosomal peptide and polyketide biosynthesis by direct detection of intermediates on > 70 kDa polypeptides by using Fourier-transform mass spectrometry. *ChemBioChem 7*, 904−907.
(26) Zettler, J., and Mootz, H. D. (2010) Biochemical evidence for conformational changes in the cross-talk between adenylation and peptidyl-carrier protein domains of nonribosomal peptide synthetases. *FEBS J. 277*, 1159−1171.
(27) Mann, M., Meng, C. K., and Fenn, J. B. (1989) Interpreting mass-spectra of multiply charged ions. *Anal. Chem. 61*, 1702−1708.
(28) Tian, Y., Suk, D. H., Cai, F., Crich, D., and Mesecar, A. D. (2008) *Bacillus anthracis o*-succinylbenzoyl-CoA synthetase: reaction kinetics and a novel inhibitor mimicking its reaction intermediate. *Biochemistry 47*, 12434−12447.
(29) Perham, R. N. (2000) Swinging arms and swinging domains in multifunctional enzymes: catalytic machines for multistep reactions. *Annu. Rev. Biochem. 69*, 961−1004.
(30) Tanovic, A., Samel, S. A., Essen, L. O., and Marahiel, M. A. (2008) Crystal structure of the termination module of a nonribosomal peptide synthetase. *Science 321*, 659−663.
(31) Kern, D., Lorber, B., Boulanger, Y., and Giege, R. (1985) A peculiar property of aspartyl-transfer RNA synthetase from bakers' yeast: chemical modification of the protein by the enzymatically synthesized aminoacyl adenylate. *Biochemistry 24*, 1321−1332.
(32) Hountondji, C., Beauvallet, C., Pernollet, J. C., and Blanquet, S. (2000) Enzyme-induced covalent modification of methionyl-tRNA synthetase from *Bacillus stearothermophilus* by methionyl-adenylate: identification of the labeled amino acid residues by matrix-assisted laser desorption-ionization mass spectrometry. *J. Protein. Chem. 19*, 563−568.
(33) Kittelberger, R., Pavela-Vrancic, M., and von Döhren, H. (1999) Active site titration of gramicidin S synthetase 2: evidence for misactivation and editing in non-ribosomal peptide biosynthesis. *FEBS Lett. 461*, 145−148.
(34) Kallow, W., von Döhren, H., and Kleinkauf, H. (1998) Penicillin biosynthesis: energy requirement for tripeptide precursor formation by delta-(L-alpha-aminoadipyl)-L-cysteinyl-D-valine synthetase from *Acremonium chrysogenum*. *Biochemistry 37*, 5947−5952.
(35) Roskoski, R., Jr., Gevers, W., Kleinkauf, H., and Lipmann, F. (1970) Tyrocidine biosynthesis by three complementary fractions from *Bacillus brevis* (ATCC 8185). *Biochemistry 9*, 4839−4845.
(36) Gulick, A. M. (2009) Conformational dynamics in the acyl-CoA synthetases, adenylation domains of non-ribosomal peptide synthetases, and firefly luciferase. *ACS Chem. Biol. 4*, 811−827.